ISBN: 978-3-95450-255-4 ISSN: 2226-0358 doi: 10.18429/JACoW-ICALEPCS2025-TUMG017

# ADAPTIVE APPROACH TO SPATIAL INTERPOLATION AND VISUALISATION OF SCATTERED MONITORING DATA AT CERN

C. M. Musso*, A. Ledeul, A. Savulescu, G. Segura Millan
CERN, Geneva, Switzerland



*Abstract*

In order to ensure safe operations, CERN leverages an extensive SCADA system to monitor radiation levels and collect environmental measurements across its premises. The Health & Safety and Environmental Protection (HSE) Unit addressed the challenge of visualising radiation fields from non-uniformly distributed sensors across large areas. This paper presents the approach and implementation of a 2D interpolation and visualisation system for such measurements. The system implements two algorithms for two complementary monitoring scenarios. The Inverse Distance Weighting (IDW) interpolation addresses cases where radiation sources are located near sensor locations, assuming maximum values occur at measurement points. The Radial Basis Function (RBF) method handles scenarios with potential measurement peaks between sensors. A region network approach divides large areas into independent regions for optimised performance. Accuracy is evaluated using leave-one-out cross-validation. The architecture relies on TypeScript, React and WebSockets. The system processes measurements across CERN's premises and provides operators with spatial visualisation of radiation levels.

## INTRODUCTION

CERN's HSE Unit operates one of the world's most important radiation monitoring systems; measuring radiological and environmental impact, ensuring workplace safety, and providing data for reporting to public and host state authorities. This monitoring infrastructure has 90 device types, manages more than 125,000 alarms, and archives around 80 billion measurements per year.

While real-time alarm systems effectively detect immediate radiation hazards, post-mortem and long term analysis requires a different approach and remains important to address. When radiation alarms occur, operators need to reconstruct the dynamics and dispersion patterns from the localised measurement values of multiple monitors. The current monitoring system provides detailed temporal data visualisation but lacks a field view for spatial interpretation of scattered sensor data.

The reconstruction of field-maps is beneficial in incident analysis, where understanding the spatial patterns of radiation fields can inform safety and operational decisions.

This paper presents an adaptive approach to spatial interpolation and visualisation of radiation monitoring data at CERN. We address two distinct monitoring scenarios that require two complementary interpolation methods: Inverse Distance Weighting (IDW) for cases where radiation sources are located at or near sensors, and Radial Basis Functions (RBF) when source locations are unknown and may exist between measurement points.

The implementation builds on established academic research: adaptive parameter selection for IDW [2] and space subdivision with adaptive shape parameter for RBF [3]. It also introduces a practical solution to numerical stability issues encountered during real scenarios testing. Similar interpolation approaches have been successfully applied to environmental monitoring in agricultural soil property mapping [4] and groundwater depth distribution analysis [5].

The system is integrated into the REMUS Web application [1], CERN's main lightweight web platform for radiation monitoring, offering a new functionality for spatial visualisation of radiation data.

## SYSTEM REQUIREMENTS AND METHODOLOGY

We establish functional requirements and interpolation strategy selection based on physical monitoring characteristics and operator workflow needs.

### *Functional Requirements*

The solution addresses a specific valuable requirement: helping operators analyse radiation distribution patterns when time series monitoring is insufficient. This becomes particularly useful during incident investigations, safety assessments, or when unusual radiation patterns appear across the monitoring region. Operators require a flexible tool that handles multiple measurement units, applies temporal data aggregation, offers interpolation method selection, and enables adjustment of sensitivity parameters and spatial resolution to meet their monitoring objectives (Fig. 1).

The system must complete processing within reasonable amount of time (seconds) and consistently deliver either a valid visualisation or an explanatory error message.

### *Interpolation Strategy Selection*

The key insight is matching interpolation methods to the physical assumptions of monitoring scenarios. When sensors are positioned on known sources, we use this additional information to apply a specific computational approach.

We distinguish two monitoring contexts. In controlled environments like CERN's ventilation systems, air is released from underground areas through conduits with sensors installed at exits; the highest value is thus assumed to be exactly at sensor location. In contrast, open monitoring areas distribute sensors across regions without predetermined pat-

* carlo.maria.musso@cern.ch

ISBN: 978-3-95450-255-4 ISSN: 2226-0358 doi: 10.18429/JACoW-ICALEPCS2025-TUMG017

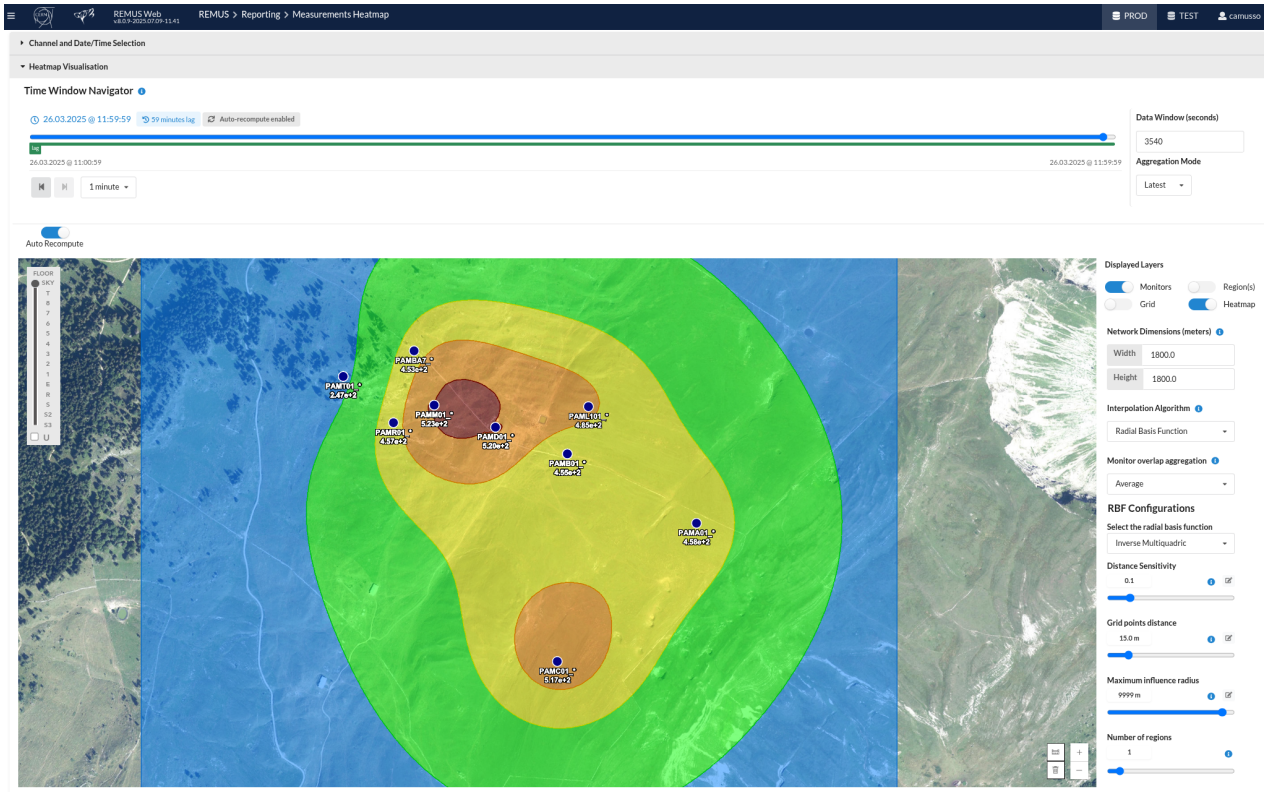


Figure 1: Monitoring interface showing time window configuration, area and layer selection controls, aggregation mode settings, interpolation algorithm parameters, and the resulting spatial visualisation of measurement data. Note: Satellite imagery is for illustrative purposes only.

terns, where peak readings may occur anywhere within the monitored space.

These scenarios directly correspond to the mathematical behaviour of different interpolation methods. IDW's conservative nature, which bounds estimates within measured values, suits known-source monitoring. RBF's capacity to extrapolate beyond measured ranges by summing sensor influences addresses unknown-source scenarios where peaks may emerge between monitoring points.

Both algorithms provide configuration parameters to adapt their behaviour to monitoring conditions and spatial characteristics, detailed in the following section.

## ARCHITECTURE AND IMPLEMENTATION

### *System Architecture*

The architecture follows a clear separation between the behaviour logic of the object classes and the React components of the user interface. The technology stack relies on Spring Boot backend, React frontend with TypeScript, WebSockets for non-blocking data communication, and d3-tricontour for the generation of radiation-level isobands.

The system is structured into two primary layers:

1. **Behaviour Layer** (`.ts`): Contains the core logic, data management, interpolation algorithms and spatial subdivision without user interface dependencies.
2. **Component Layer** (`.tsx`): Contains React-based user interface elements that render data and capture user interactions, including configuration panels, map visualisation, and analytics displays.

The data manager coordinates measurement loading and processing while the processor handles unit conversion and normalisation before feeding data to interpolation algorithms.

The data pipeline follows this sequence: WebSocket subscription → Data loading → Normalisation → Spatial analysis → Interpolation → Visualisation rendering (Fig. 2). Raw measurements are filtered by time window, aggregated using user-selected methods, converted to common units, and normalised to [0-1] range before interpolation.

### *Adaptive IDW Implementation*

The IDW implementation builds upon Lu and Wong's adaptive methodology [2]. The fundamental principle of IDW expresses how measured values influence the grid points (where we predict radiation levels) through an inverse relationship with distance:

$$v(\mathbf{x}) = \frac{\sum_{i=1}^{n} w_i \cdot v_i}{\sum_{i=1}^{n} w_i} \quad (1)$$

where $v(\mathbf{x})$ is the interpolated value at location $\mathbf{x}$, $v_i$ is the measured value at sensor $i$, $w_i$ is the weight assigned to

ISBN: 978-3-95450-255-4 ISSN: 2226-0358 doi: 10.18429/JACoW-ICALEPCS2025-TUMG017

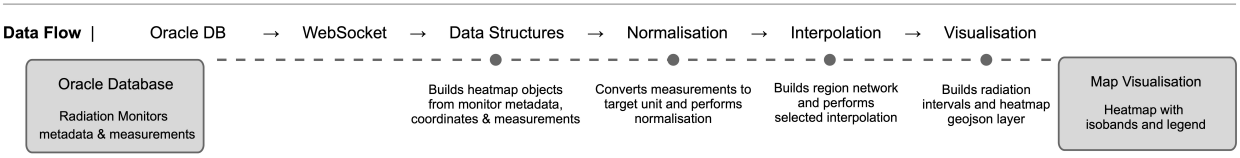


Figure 2: Data flow from Oracle database to visualisation.

sensor $i$, and $n$ is the number of sensors. The weights are defined as:

$$w_i = \frac{1}{d(\mathbf{x}, \mathbf{x}_i)^p} \tag{2}$$

where $d(\mathbf{x}, \mathbf{x}_i)$ is the Euclidean distance between the interpolation point $\mathbf{x}$ and sensor location $\mathbf{x}_i$, and $p$ is the power parameter that controls the rate of distance decay.

The adaptive approach [2] dynamically adjusts the power parameter $p$ based on spatial pattern analysis. The system detects if sensors are clustered, random, or dispersed by computing nearest-neighbour statistics, then maps these values to appropriate $p$ values. Clustered patterns receive smaller $p$ values (broader influence), while dispersed patterns get larger $p$ values (localised influence).

### *RBF with Space Subdivision*

The RBF implementation follows Smolik and Skala's approach [3] with space subdivision. The interpolating function is constructed as:

$$f(\mathbf{x}) = \sum_{i=1}^{n} w_i \cdot \phi(||\mathbf{x} - \mathbf{c}_i||) \tag{3}$$

where $f(\mathbf{x})$ is the interpolated value at point $\mathbf{x}$, $w_i$ are the weights to be determined, $\phi$ is the radial basis function, $\mathbf{c}_i$ represents the sensor locations, and $||\mathbf{x}-\mathbf{c}_i||$ is the Euclidean distance between the interpolation point and sensor $i$.

Common radial basis functions include:

- **Gaussian**: $\phi(r) = e^{-(\varepsilon r)^2}$
- **Inverse multiquadric**: $\phi(r) = \frac{1}{\sqrt{1+(\varepsilon r)^2}}$
- **Inverse quadric**: $\phi(r) = \frac{1}{1+(\varepsilon r)^2}$

where $r$ is the distance and $\varepsilon$ is the shape parameter that controls the width of the radial basis function.

Weight determination requires solving the matrix system $\mathbf{\Phi w} = \mathbf{z}$ where $\mathbf{\Phi}$ is the interpolation matrix containing influence values between all sensor pairs, $\mathbf{w}$ is the vector of weights, and $\mathbf{z}$ is the vector of measured values. Regional decomposition divides the spatial domain into subregions, preventing numerical instability arising from large disparities in inter-sensor distances. Each region optimises its shape parameter $\varepsilon$ based on sensor distribution. The system also ensures smooth transitions between boundaries by keeping track of neighbouring regions and extending each region's interpolation to its overlapping boundaries. Points on boundaries are computed using contributions of all overlapping regions.

### *IDW and RBF Visualisation Characteristics*

The fundamental mathematical differences between IDW and RBF interpolation methods produce different spatial visualisations. IDW shows circular decay patterns centred at sensor locations, where interpolated values are bounded by the measurement range and maxima occur at sampling points. This behaviour comes from IDW's weighted average approach, where influence decreases with distance according to the inverse distance relationship. In contrast, RBF's function approximation method, allowing superposition of radial influences, creates visualisations where peaks emerge between sensor locations. Figure 3 illustrates these distinct visualisation patterns applied to the same radiation monitoring scenario.

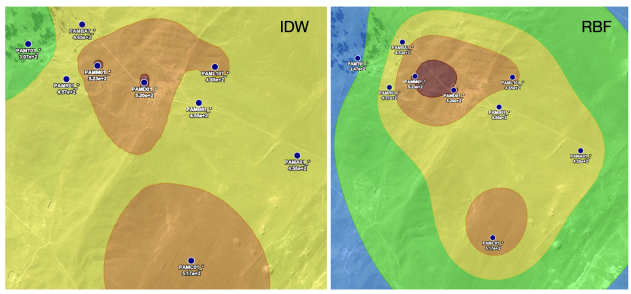


Figure 3: IDW (left) and RBF (right) interpolation of the same scenario, demonstrating the distinct visualisation patterns described above.

### *Configuration Parameters*

Both interpolators share common parameters: *Distance Sensitivity* controls how rapidly sensor influence decreases with distance (0-1 range), applied after interpolation; 0 meaning no additional distance-based reduction, 1 representing maximum limitation of extrapolated values, constraining predictions to areas close to sensors.

*Grid Step* sets interpolation resolution as a percentage of region size, controlling the density of points where radiation values are estimated. *Sensor Overlap Aggregation* determines the method used to combine measurements when multiple sensors occupy identical locations (average, median, min, max).

RBF includes additional parameters: *Function Type* selects between different radial basis functions, and *Number of Regions* controls spatial subdivision with options for 1, 4, or 16 regions.

ISBN: 978-3-95450-255-4 ISSN: 2226-0358 doi: 10.18429/JACoW-ICALEPCS2025-TUMG017

The system incorporates safety checks and constraints to prevent unstable configurations and provides explanatory error messages when calculations fail.

### *New Hybrid Approach*

The hybrid approach [6] addresses numerical instability issues encountered during RBF implementation with real-world monitoring data. While region subdivision handles scenarios with excessive ratios between nearest and farthest sensor distances, RBF remains vulnerable to instability when closely positioned sensors report conflicting measurements.

When triggered, the hybrid method implements a reduced IDW interpolation as a preprocessing step. The system constructs a dense grid (0.1% of region size) and selects the nearest grid point for each sensor. These grid points then undergo IDW interpolation, which encodes monitor values into stable grid-point estimates.

This preprocessing step resolves proximity conflicts by mapping closely positioned sensors to the same grid point, thus merging their conflicting measurements into a single value. The resulting stabilised grid points then serve as input to the RBF algorithm. The very dense grid (0.1% resolution) preserves sensor values accurately, with almost no loss of information for the RBF interpolation.

This hybrid approach maintains numerical stability in RBF interpolation even when neighbouring sensors disagree on measured values, avoiding ill-conditioned matrices in the underlying system of equations that RBF is solving, and thus providing a more robust interpolation.

## EVALUATION AND RESULTS

The approach was tested on a real-world scenario proposed by a CERN operator in radiation protection, using background radiation data to validate interpolation accuracy. The measurement values were normalised to generalised units to preserve data sensitivity while maintaining relative proportions for comparable evaluation.

### *Test Dataset and Methodology*

The evaluation employed measurements from 39 radiation monitors distributed across 1 km$^2$ of CERN's surface installations, consolidated to 9 unique spatial locations after median value aggregation (Fig. 4).

Leave-one-out cross-validation removes each sensor and predicts its value using the remaining eight sensors. Four metrics evaluated interpolation accuracy: Mean Absolute Error (MAE), Median Absolute Error (MedAE), Mean Absolute Percentage Error (MAPE), and Median Absolute Percentage Error (MedAPE).

The resulting field map from RBF execution can be seen in Fig. 5. RBF with inverse multi-quadric function showed the following accuracies according to sensor dispersion:

Six sensors achieved accuracy above 85%, while three sensors performed below 70%. This shows RBF accuracy varies significantly depending on sensor dispersion, as illustrated in Fig. 6 which shows accuracy per single sensor removed.

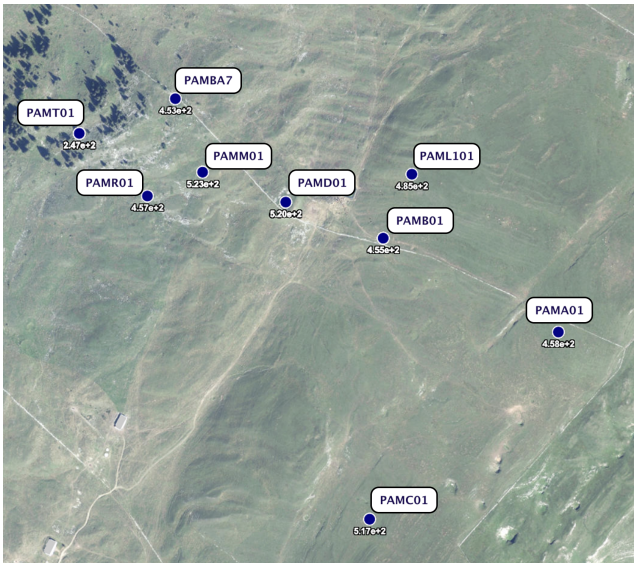


Figure 4: Scenario on which tests were performed.

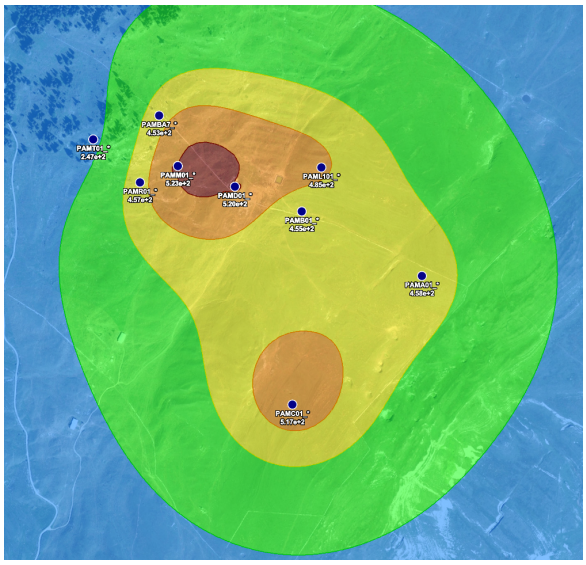

Figure 5: RBF interpolation - Computation time: 38 ms.

The overall metrics are summarised in Table 1.

Table 1: Overall RBF Performance Metrics

| Metric | Value |
|---|---|
| MAE | 74.22 |
| MedAE | 47.00 |
| MAPE | 17.53% |
| MedAPE | 9.63% |

The median error is much lower than the mean error, which tells us an important fact: most predictions work reasonably well, but a few very bad predictions pull error averages up.

ISBN: 978-3-95450-255-4 ISSN: 2226-0358 doi: 10.18429/JACoW-ICALEPCS2025-TUMG017



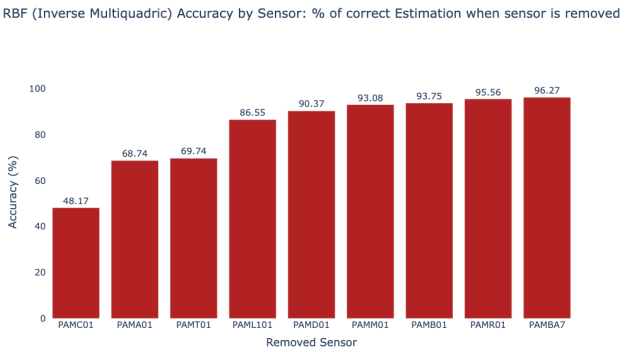


Figure 6: RBF (Inverse Multiquadric) accuracy by sensor: percentage of correct estimation on sensor removal.

The pattern becomes clear when we look at which sensors had poor prediction accuracy. Three sensors (PAMC01, PAMA01, PAMT01) are located in areas with sparse sensor coverage.

When we remove one of these more isolated sensors, the interpolation algorithm must estimate its value using only distant sensors. This reveals a fundamental limitation of interpolation methods: they require adequate sensor coverage, with reliability dropping significantly in sparsely monitored areas.

### *Performance and Configuration Impact*

Grid step size represents the primary computational trade-off. Dense grids (0.5% of region size) require approximately 290 ms computation with 40,100 interpolation points, providing detailed visualisation. Sparse grids (8%) complete in under 5 ms with 250 points but sacrifice spatial resolution. The performance comparison across different configurations is presented in Table 2.

Table 2: RBF Interpolation Performance Comparison

| Config | Time (ms) | Perf. | Points |
|---|---|---|---|
| Dense (0.5%) | 290 | 1x | 40100 |
| Default (3%) | 31 | 9.35x | 2400 |
| Sparse (8%) | 5 | 58x | 250 |
| Hybrid Dense | 462 | 1x | 9+40100 |
| Hybrid Default | 57 | 8.1x | 9+2400 |
| Hybrid Sparse | 16 | 28.8x | 9+250 |

The distance sensitivity parameter lets operators control how much to trust measurements from distant sensors, allowing them to balance between relying on distant readings or focusing predictions on areas close to sensors. Performance characteristics support monitoring requirements with standard configurations completing within seconds.

## CONCLUSION

We developed a robust radiation visualisation system for CERN's environmental monitoring department by adapting established academic interpolation methods—Lu & Wong's adaptive IDW and Smolik & Skala's RBF techniques [2, 3]—for practical monitoring applications. We also developed a hybrid approach that prevents numerical instability when sensors report inconsistent measurements at close distances.

Testing on actual CERN data showed the system works reliably for most sensors, though accuracy drops in areas with sparse coverage—an inherent limitation of any interpolation method. The system runs fast enough and provides the spatial visualisation capabilities that CERN operators needed for incident analysis.

This approach offers a practical framework for creating spatial visualisations of radiation monitoring data. Its versatile, system-agnostic design makes the software readily applicable to other contexts, including CERN's Noise Monitoring program.

## ACKNOWLEDGEMENTS

We would like to thank all the members, past and present, of the REMUS team as well as colleagues from Radiation Protection, Environment, Engineering, Information Technology and Control departments for their fundamental contribution to the success of the REMUS project.

We extend our deepest gratitude to the HSE-TS-CS team for their excellent development of REMUS Web, which made possible the straightforward integration of our interpolation system, and to CERN's GIS department for the support and infrastructure they provided for this research.

## REFERENCES

[1] A. Ledeul, A. Savulescu, and G. Segura, "Web Dashboards for CERN Radiation and Environmental Protection Monitoring," in *Proc. ICALEPCS'23*, Cape Town, South Africa, Oct. 2023, pp. 938–943. doi:10.18429/JACoW-ICALEPCS2023-TUSDSC07

[2] G. Y. Lu and D. W. Wong, "An adaptive inverse-distance weighting spatial interpolation technique," *Comput. Geosci.*, vol. 34, no. 9, pp. 1044–1055, 2008. doi:10.1016/j.cageo.2007.07.010

[3] M. Smolik and V. Skala, "Large scattered data interpolation with radial basis functions and space subdivision," *Integr. Comput.-Aided Eng.*, vol. 25, no. 1, pp. 1–14, Nov. 2017. doi:10.3233/ICA-170556

[4] C. G. Karydas, I. Z. Gitas, E. Koutsogiannaki, N. Lydakis-Simantiris, and G. N. Silleos, "Evaluation of spatial interpolation techniques for mapping agricultural topsoil properties in Crete," *EARSeL eProceedings*, vol. 8, no. 1, pp. 26–39, 2009.

[5] K. H. Yasin, T. B. Gelete, A. D. Iguala, and E. Kebede, "Optimal interpolation approach for groundwater depth estimation," *MethodsX*, vol. 13, pp. 102916, Aug. 2024. doi:10.1016/j.mex.2024.102916

[6] C. M. Musso, "Radiation Monitoring: a Robust Approach to Spatial Visualisation of Sensor Data," Masters thesis, École Polytechnique Fédérale de Lausanne, 2025.